Physics at a future linear e^+e^- collider

Alexei Raspereza
DESY Hamburg
Notkestrasse 85, D-22607 Hamburg, Germany

Abstract

The International Linear Collider (ILC) has a rich physics program, providing an experimental tool for exploration of electroweak symmetry breaking mechanism and investigation of theories beyond the Standard Model (SM). If there is a light Higgs boson the Large Hadron Collider (LHC) is expected to discover it, but the ILC will be able to precisely determine the profile of such a particle. Moreover, the the extended Higgs sector predicted by supersymmetric extension can be established. If supersymmetric particles appear, the ILC will measure a set of them complementary to those observed at the LHC, and may allow extrapolation of supersymmetric parameters to the GUT scale. If strong electroweak sector is indicated, the ILC will be able to reveal the structure of the strong electroweak symmetry breaking. In addition, the ILC is expected to have sensitivity to models postulating extra spatial dimensions. Finally, the anticipated precision of electroweak observable measurements will give an insight into new physics at very large energy scales through virtual effects. In this paper, the features of the machine are outlined, the detector concept is discussed and the physics potential of a linear collider is reviewed.

1 Introduction

Over the last few years a consensus has emerged within the particle physics communities worldwide that the next big machine to be built should be an electron-positron linear collider, operating at energies between a few hundred GeV and approximately one TeV. In a series of international workshops the physics community has evaluated both the physics program at such a machine and the resulting requirements that must be met by both the machine and detector in order to reach the established physics goals. They have been documented among others in the TESLA Technical Design Report [1], the SNOWMASS Report [2] and the JLC roadmap book [3]. The agreement achieved based upon a long and successful history of particle physics. A large amount of data collected at machines such as LEP, HERA, the Tevatron and B factories allowed to establish and test the Standard Model, the theory which describes the strong, electromagnetic and weak interactions.

Starting in 2007, the Large Hadron Collider (LHC) will continue investigation of the SM and search for new physics. It is hoped that the last missing piece of the SM puzzle, the Higgs boson, will be discovered and light will be shed upon the mechanism of the electroweak symmetry breaking. It is also expected that the first indications of possible new physics beyond the SM will be found. The LHC will be the first machine which will push the energy scale well beyond the electroweak scale, close to the TeV energy scale.

However, the LHC by itself will not be able to reveal completely the mechanism of electroweak symmetry breaking. It should be complemented by collider operating at energies close to one TeV. Such a machine will investigate in detail the structure of electroweak sector and study the Higgs boson, if it exists. In addition, nearly all scenarios beyond the Standard Model will have observable signatures at the linear collider, making such a machine an ideal tool to study new physics in a way complementary to the LHC. In this article a review of the physics potential of a future linear collider is presented. The paper is organized as follows. First, the machine features will be outlined in a separate chapter, followed by section discussing in details the detector concept considered for the linear collider. Then an overview of the physics program at the linear collider will be given. A brief summary will conclude the paper.

2 Machine

The LEP collider approached the technical frontier for a circular electron accelerator. The energy loss of the accelerated electrons per turn due to synchrotron radiation is $\Delta E \sim E_b^4/R$, where E_b is the beam energy and R is the radius of the accelerator. At highest LEP energies, these energy losses reached several GeV per turn, thus limiting maximal attainable energy to approximately 200 GeV. In order to reach sub-TeV energy scales, a future e^+e^- collider must be realized as a linear accelerator since for such a machine no energy losses due to synchrotron radiation exist.

The advantages of an e^+e^- collider, in comparison to a proton machine, are a well defined initial state and the possibility to tune both center-of-mass energy and polarization of electrons and positrons very precisely. Moreover, e^-e^-, $e^-\gamma$ and $\gamma\gamma$ collision option are foreseen extending physics potential of such a collider. It is planned that in the first phase, the machine will operate at center-of-mass energy of a few hundred GeV, thus covering the scale of electroweak symmetry breaking. The machine will then be upgraded to the energy of approximately 1 TeV to extend the discovery potential of the collider.

Two technologies have been proposed for a future linear e^+e^- collider. One of the technologies is based on cold superconducting acceleration concept. This project was developed at DESY and is known under the name TESLA (Tera Electronvolt Superconducting Linear Accelerator). The alternative approach utilizes conventional warm technology and has been developed in North America and Asia. This option is known under the name NLC (Next Linear Collider) machine. Technical characteristics of both colliders are summarized in Table 1.

Parameter	NLC	TESLA
Energy reach, GeV	500−1000	500−800
Interbunch separation, ns	1.4	180−340
RF frequency, GHz	11.4	1.3
Bunches per train	192	2820−4890
AC power, MW	200−300	100−160
Bunch transversal size σ_x/σ_y, nm	220−250/2−3	400−550/3−5
Bunch longitudinal size σ_z, μm	110	300
Particles per bunch	$0.8\cdot10^{10}$	$(1.4-2)\cdot10^{10}$
Luminosity, $cm^{-2}s^{-1}$	$(2-3)\cdot10^{34}$	$(3.4-5.8)\cdot10^{34}$

Table 1: Technical characteristics of the two options of the linear e^+e^- collider [4].

The key difference between the two options is the structure of the beams. At cold superconducting machine accelerated particles are grouped into trains each containing several thousand bunches separated by few hundred ns. At a warm machine due to higher RF frequency, the number of bunches is reduced to about 200 hundred, but bunches are separated by only 1.4 ns. This difference has important implications for physics performance. Apart from a number of advantages, the linear collider has few unpleasant features. One of these is beamstrahlung, the process of photon radiation by electron/positron against the electromagnetic field produced by a dense opposite bunch. This will have a negative impact on the physics performance of the collider.

First, beamstrahlung will distort the energy spectrum of the colliding beams. As a consequence, initially nearly monochromatic beams will be characterized by the energy spectrum containing long tail extending to very low energies. This is illustrated in Figure 1 Thus, no precise information of center-of-mass energy of colliding particles will be available on an event by event basis. But the most serious consequence of beamstrahlung is associated to the interactions of beamstrahlung photons. These lead, for example, to the creation of lepton pairs. Approximately $1.5\cdot10^5$ lepton pairs with $E > 5$ MeV per bunch crossing are expected in both cold and warm machines [4]. In most of the cases, leptons escape undetectable into beam pipe or can be efficiently tagged with very forward detectors. However, a more dangerous background comes from hadronic interactions of beamstrahlung photons. About one such an event per ten bunch crossings is expected at both machines [4]. Hadronic interactions of beamstrahlung photons may overlap with physics events, diluting the signatures of the processes to be studied at the linear collider. This implies very stringent requirements for the time-stamp capabilities of the detector at the warm machine. Even if the detector were capable of resolving beam-beam interactions with the time resolution of 10 ns, this would mean that there will be in average one hadronic interaction overlaid with one physical event. It was shown that even under this rather optimistic assumption, the physics performance will be considerably deteriorated [5].

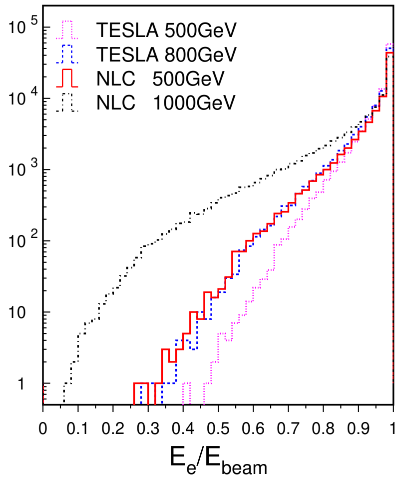

Figure 1: The spectrum of colliding particle energy normalized to the energy of the beam undistorted by beamstrahlung for TESLA machine operated at $\sqrt{s}$ = 500 GeV (dotted line), TESLA machine operated at $\sqrt{s}$ = 800 GeV (dashed line), NLC machine operated at $\sqrt{s}$ = 500 GeV (continuous line) and NLC machine operated at $\sqrt{s} = 1$ TeV (dashed-dotted line).

Since, for cost reasons realization of the two technologies seems not to be possible, the International Technology Recommendation Panel (ITRP) was appointed which included representatives from North America, Europe and Asia. The task of ITRP was to assess physics implication of the linear collider technology choice and formulate a recommendation on technology for the linear collider. In August 2004, ITRP made an official statement in which it recommended cold technology and urged particle physics communities worldwide to unite behind this project. Reasons for this choice are summarized in Final ITRP Report [6].

3 Detector

The detector performance motivated by the planned physics program at the linear collider can be summarized in the following requirements:

- excellent momentum resolution in the central tracking system to determine the recoil mass with optimal resolution;
- very high b- and c-tagging efficiency to identify multi-b final states, e.g ZZH and $t\bar{t}H$, and to measure precisely the Higgs boson branching fractions $H \to b\bar{b}$ and $H \to c\bar{c}$;
- good hermeticity to enable accurate measurement of missing energy and therefore provide sensitivity to the SUSY signatures;
- good momentum resolution in the forward region to identify charges unambiguously down to lowest angles and up to highest momenta and very good angular resolution in this region to measure the luminosity spectrum from the acolinearity of Bhabha events;
- very good pattern recognition capabilities to find tracks within jets in the high track density environment;
- good imaging capabilities of the calorimeters in order to separate photons and neutral hadrons from charged particles within jets with very high local particle density;
- calorimeter design enabling reconstruction of photons non-pointing to the IP in order to provide sensitivity to some of the SUSY signatures.

The relation between detector performance and the physics goals will be discussed in detail in the section dedicated to the physics program at the linear collider.

Three detector concepts are currently being developed for the linear collider experiments. These are the "huge", "large" and "small" detector concepts which are studied worldwide. The main difference between the three concepts is the size and option for the tracking system. Within the "huge" and "large" detector concepts, the main part of the tracking system is represented by a large volume gaseous detector, supposedly a Time Projection Chamber (TPC), in which good momentum resolution and high tracking efficiency are achieved by a large number of measurement points within the gas volume. The "huge" detector implies a somewhat large radius of the tracking device. An alternative tracker option foreseen for the "small" detector is based on few layers of Si strip detectors arranged in cylinders to fill the space between the vertex tracker and calorimeter [7]. Based on studies done for the LHC experiments, it is expected that the excellent resolution obtainable with these devices compensates for the fact that there are only few points, maintaining a good tracking efficiency.

All three concepts are the subject of extensive R&D studies aiming to find a compromise between the detector performance and cost. Let us consider as an example the TESLA detector, which has become a baseline benchmark for a "large" detector concept. The detector, of which a quarter is depicted in Figure 2, follows in general the structure of the LEP detectors.

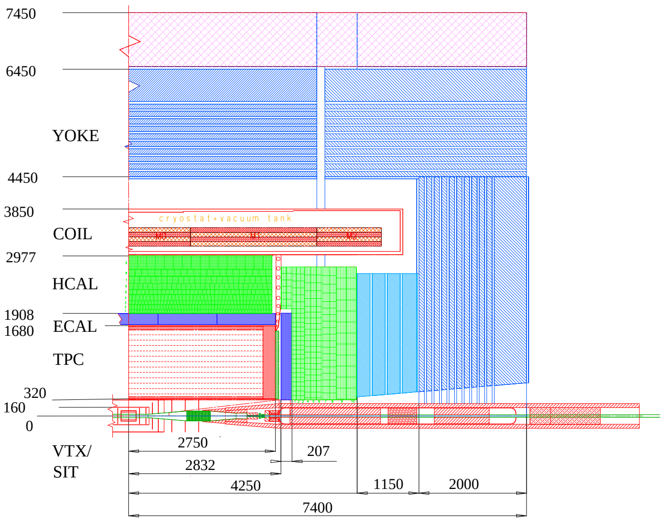

Figure 2: The view of a quadrant of the TESLA detector.

Starting from the interaction point there is a silicon tracker, including vertex detector (VTX) and Silicon Intermediate Tracker (SIT), a Time Projection Chamber as a main tracking device. In the radial direction follow electromagnetic (ECAL) and hadron calorimeters. To ensure good track reconstruction for charged particles produced at lower polar angles, tracking system is complemented by silicon discs (FTD) and forward chambers (FCH) implemented as straw-tubes. All these subdetectors are placed in a superconducting solenoidal magnet producing magnetic field of 3−4 T. The return yoke plates interleaved with active sensors (resistive plate chambers or scintillating tiles) perform the function of the muon system. The very forward region is instrumented with a Low Angle Tagger (LAT) and a luminosity calorimeter (LCAL). The detector is equipped with a tungsten mask shielding detector from backward scattered particles produced by the interaction of beamstrahlung photons and e^+e^--pairs with focusing quadrupole magnets.

In the following, the review of the main detector components is presented.

3.1 Microvertex Detector

The detector closest to the interaction point is the vertex detector, which is constructed from Si pixel detectors. The vertex detector is designed to provide precise track reconstruction of the secondary vertices in the proximity of the interaction point and hence facilitate the efficient c- and b-tagging. A number of different technologies are under discussion for this detector, namely CCD sensors, CMOS sensors and other options. The common feature of the proposed technologies is that they are based on pixel devices of size not larger than 50×50 μm. This is to ensure that occupancy of such detectors during operation stays below a few percent. At first sight, the average impact parameter of a B decay product, approximately 300 μm for boost $\beta\gamma > 3$, suggests that modest detector performance would be sufficient. However this is misleading. Firstly, the average impact parameter for τ and charm particle decay products are 3−4 times smaller. Equally important is the correct assignment of nearly all tracks to primary, secondary and tertiary vertices and therefore accurate determination of the vertex mass and charge which permit greatly improved b/c separation. This mandates a more advanced design of the vertex detector with respect to those used in currently ongoing experiments at B-factories. To illustrate this, Figure 3a compares c- and b-tagging performance of the vertex detectors with 4 and 5 layers as evaluated by dedicated simulation studies [8]. For particles produced at polar angle of 90^o, the envisaged impact parameter resolution of the 5-layer CCD detector, depicted in Figure 3b, is $\sigma_{IP} = 2.7 \oplus 3.9/(p \cdot \sin^{3/2}\Theta)$ [9].

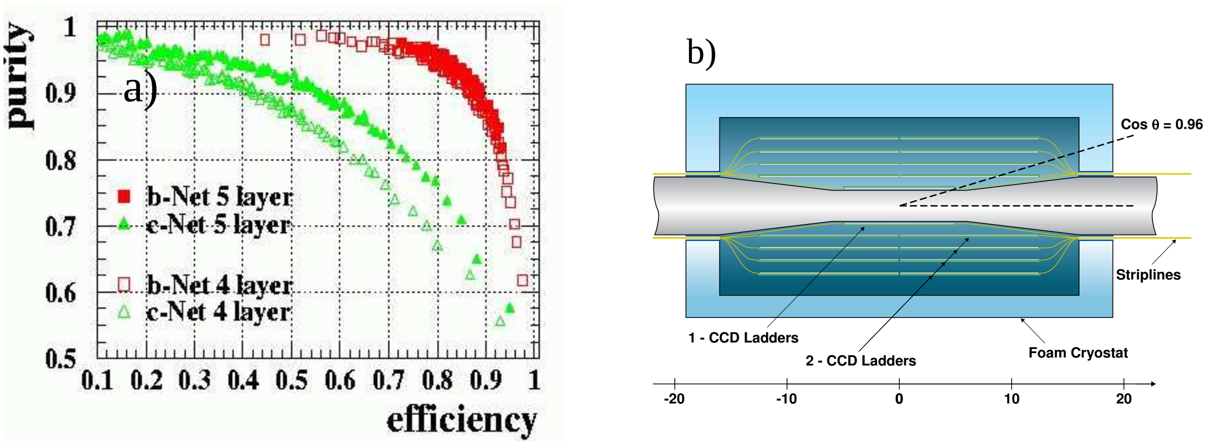

Figure 3: Purity vs. efficiency of the c- and b-tagging for the detector with 4 and 5 layers of Si sensors (left plot). Dependence is obtained for the sample of hadronic events at the Z pole. The view of CCD detector with 5 layers (right plot).

3.2 Central Tracking System

A benchmark condition driving the design of the main part of the tracking system is that the momentum resolution should be such that the mass resolution achieved for the recoiling muons in the reaction $HZ \to H\mu^+\mu^-$ is not dominated by detector effects [10].

The large volume TPC, a sketch of which is depicted in Figure 4, seems to be an optimal choice to meet the benchmark requirement mentioned above. This device has the following advantages:

- possibility of tracking to large radius which will enable reconstruction of the long lived particle decays;
- track reconstruction with many space-points and with good point resolution ($\sim$ 100 μm);
- true 3D reconstruction (1 time, 2 space coordinates);
- gaseous detector introduces low material budget;
- possibility of particle ID through the measurement of specific ionisation loss dE/dx.

The important issue in designing a TPC is the readout technology. Currently, micro-gas detectors such as GEMs (Gas Electron Multipliers) and micromegas are considered as the most promising technologies for the TPC readout. Such devices have a number of advantages in comparison with conventional wire readout. These advantages are described in detail in the TESLA Technical Design Report [1].

Simulation studies have shown that for the overall tracking system foreseen for the "large" TESLA like detector, the track momentum resolution of $\delta p_t/p_t^2 \sim 5{\cdot}10^{-5}$ (GeV/c)$^{-1}$ is feasible.

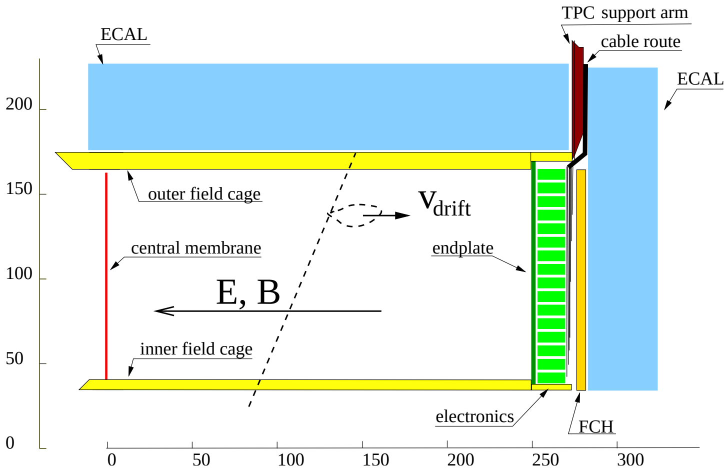

Figure 4: A sketch of the TPC volume. The electric field is applied parallel to the magnetic field. The induced electron clouds drift away from the central membrane (cathode plane) along the z axis. The $r\phi$ coordinates are determined with readout pads collecting amplified charge at the TPC endplate. The z coordinate is reconstructed by the drift time.

3.3 Calorimeters

The physics program for the planned collider demands extremely sophisticated types of measurements ranging from the reconstruction of every single particle in an event, both isolated and within the high local particle density environment to the reconstruction of event properties such as the jet structure in multijet events. Given this ambitious goal, the calorimetric system should have good pattern recognition capabilities to enable separation of close-by showers. This is possible if calorimeters are realized as devices with high longitudinal and transverse segmentation. The ideal electromagnetic calorimeter can be viewed as a sampling detector with a typical size of the cell given by the Moliere radius of the material. If it is supplemented by many samples along the direction of the shower development, a detailed reconstruction of individual showers becomes possible. A tungsten sampling calorimeter seems to be an optimal choice for the ECAL. Most of the current studies consider Si pads as the best option for an active media of such a calorimeter. Si detectors are thin, easy to segment into small cells and can be produced to cover large areas. The anticipated energy resolution of the ECAL is $\Delta E/E \sim 10\%/\sqrt{E}$.

Compared to the electromagnetic calorimeter, the reconstruction with a hadronic calorimeter is in some respect more challenging, since the presence of neutrons in a hadronic shower results in a much less localized nature of the shower. Furthermore, a good hadronic calorimeter should be able not only to reconstruct the hadronic part of the shower but also identify the electromagnetic component in each shower. At the moment two different concepts for the HCAL are being studied. The more conventional approach is based on the sampling calorimeter utilizing a scintillator readout element to determine the position and amplitude of the energy deposits. A different option puts emphasis on the spatial information by reading out the calorimeter in an extremely fine grained way, but only recording whether a cell was hit or not. The second approach, referred usually to as digital calorimetry, allows also to reconstruct the energy of showers as the number of hit cells is nearly proportional to the particle energy [1]. The most favoured option for the digital HCAL is based on resistive plate chambers as readout elements. Nonetheless other approaches e.g. with GEM based readout are also being investigated. In both digital and analog design, few cm thick steel plates are viewed as a baseline option for absorber layers. Typical cell sizes considered for the analog tile HCAL are around 5×5 cm^2. Nonetheless, it has been shown that shower separation performance of the analog HCAL can be greatly improved by decreasing cell size from 5×5 down to 3×3 cm^2 [11]. It is, however, unclear if such a finely granulated tile HCAL can be built, as the reduction of tile size leads to increase in the number of readout channels, thus raising the overall cost of the detector. The readout of a correspondingly large number of channels presents a significant challenge. Conventional photo-tubes are disfavoured because of cost and their inability to operate in a strong magnetic field. The principal feasability of a novel approach has been recently demonstrated [12] whereby Si-based tiny photo-multipliers are attached directly to the tiles. Such devices offer around 1000 pixels in a 1 mm^2 area, with each pixel operating in the Geiger mode. The number of fired pixels serves

[1] This statement is true for typical particle energies within hadronic jets, E < 10 GeV. For higher energies the dependence of the number of hit cells on the incident particle energy becomes non-linear.

as a measure of the amout of produced scintillating light and hence quantifies the deposited energy. The digital HCAL option requires a readout system which can record the "fired" cells of typically 1×1 cm^2 over large areas. The envisaged energy resolutions of the HCAL for single hadrons is $\Delta E/E \sim 30\%/\sqrt{E}$.

4 The Particle Flow Concept and Event Reconstruction

The most promising strategy for event reconstruction in the future linear collider experiment is based on the particle flow concept, implying reconstruction of the four-vectors of all particle produced in an event. The particle flow algorithm works best at moderate energies of individual particles, below about 100 GeV. In this regime, the tracking system reconstructs the momentum of the charged particles with an accuracy which can be achieved for the energy and angle measurements with calorimeters (see Figure 5). Hence, in order to attain a better reconstruction of events, the charged particle measurement must be solely based on the tracking information. The crucial step of the particle flow algorithm is correct assignment of calorimeter hits to the charged particles and efficient separation of close-by showers produced by charged and neutral particles. A clustering algorithm is then performed on calorimetric hits not assigned to the charged particles to reconstruct photons and neutral hadrons. The reconstruction of photons and neutral hadrons buried in jets is nearly impossible with a typical LEP detector. This explains why LEP detector could reconstruct jet energy with something like $60\%/\sqrt{E}$. The goals of the physics program at the linear collider requires however much better jet energy resolution in order to efficiently separate e.g. ZZ and WW final states. Monte Carlo studies have shown that an ideal reconstruction algorithm [13], which finds each particle and measures its energy and direction with the detector resolution expected for single particles, could reach a jet energy resolution of $14\%/\sqrt{E}$. Over the years a jet energy resolution of $14\%/\sqrt{E}$ has become accepted as a good compromise between the theoretically possible and practically achievable resolution. The SNARK package [14], recently developed at DESY, represents the first software implementation of the particle flow concept. A good performance of this implementation was demonstrated in a number of Monte Carlo studies[13, 15]. As an example, Figure 6 illustrates the capability of the SNARK package to reconstructed complicated event topologies such as the six jet final state resulting from the top quark pair production process, $t\bar{t} \to W^+bW^-\bar{b}$.

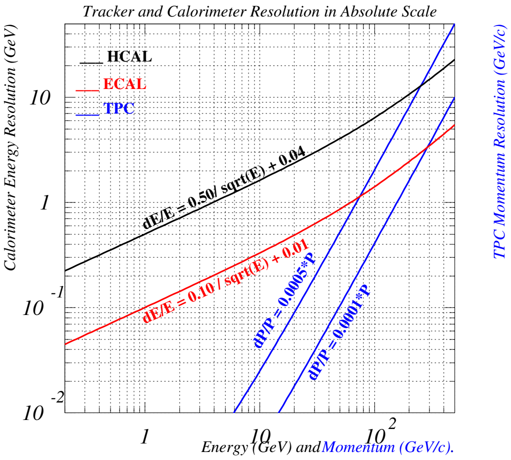

Figure 5: The track momentum resolution for charged objects and the energy resolution for photons and hadrons as a function of particle energy.

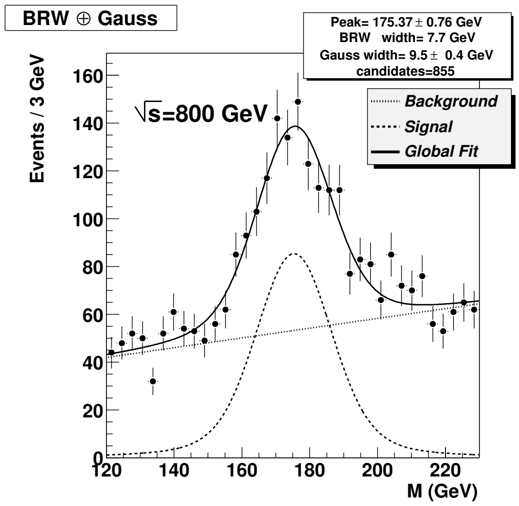

Figure 6: The distribution of the reconstructed top quark mass in the selected sample of the $t\bar{t} \to W^+bW^-\bar{b}$ events [15]. The center-of-mass energy is 800 GeV. Assumed integrated luminosity is 300 fb^{-1}.

5 Physics at the ILC

In this section, the physics potential of the e$^+$e$^-$ linear collider will be discussed. It is hard to highlight the entire physics program at such a machine. Hence, the emphasis will be put on few selected key topics: Higgs mechanism, supersymmetry, extra spatial dimensions and strong electroweak symmetry breaking.

5.1 Higgs mechanism

The central task of the physics program at the e$^+$e$^-$ linear collider focuses on the detailed study of the structure of the electroweak symmetry breaking. Nowadays the most favored scenario is the Higgs mechanism. If the Higgs boson exists, it will most likely be detected at the LHC. Following this discovery, a linear collider will accurately reconstruct the Higgs boson profile. Two main Higgs boson production mechanisms are the Higgs-strahlung and WW/ZZ fusion processes. Cross sections of these processes as a function of the Higgs boson mass are displayed in Figure 7. The decay properties of the Higgs boson depend on its mass. At a Higgs boson mass below about 130 GeV, the main decay mode is $H \to b\bar{b}$. At higher masses the decay into W pairs takes over. Figure 8 shows the dependence of the Higgs boson branching ratios on the Higgs boson mass and demonstrates precision with which branching ratios can be measured at the linear collider.

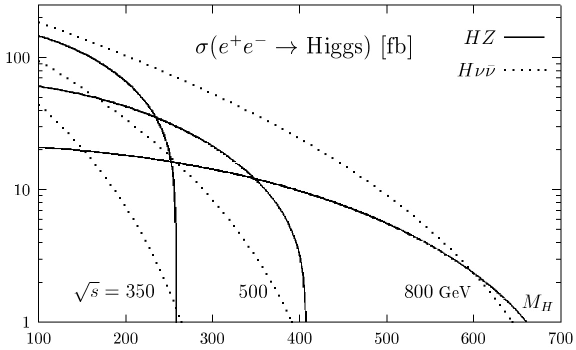

Figure 7: The SM Higgs boson production cross sections as a function of the Higgs boson mass.

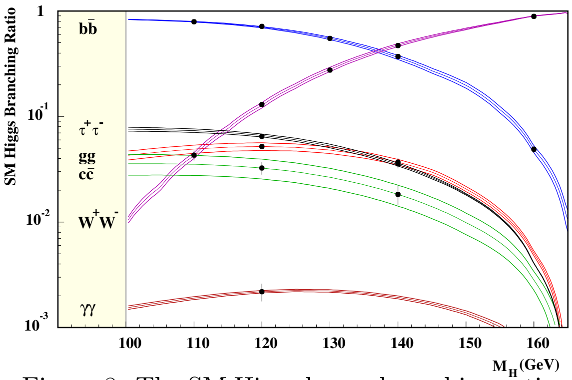

Figure 8: The SM Higgs boson branching ratios as a function of the Higgs boson mass. Points with error bars show the expected experimental accuracy, while the lines show the estimated uncertainty on the theoretical predictions.

The main advantage of the linear collider is its capability to detect the Higgs boson independently of the Higgs boson decay mode due to clean experimental environment. Even within the exotic scenarios predicting the dominance of the Higgs production into invisible particles, for example a pair of the lightest neutralino, the observation of the Higgs boson will be possible by analyzing the mass spectrum of the system recoiling against lepton pair in the process $HZ \to X\ell^+\ell^-$ where ℓ is either electron or muon. This is illustrated in Figure 9. In addition, the recoil mass analysis provides the tool for model independent measurement of the Higgs-strahlung cross-section. Dedicated studies [16] have shown that the Higgs-strahlung cross-section can be measured with an accuracy of 2.6% to 3.1% for Higgs masses from 120 to 160 GeV assuming 500 fb^{-1} of integrated luminosity collected at an energy of 350 GeV. The mass of the light Higgs boson can be determined exploiting the $HZ \to b\bar{b}q\bar{q}$, $HZ \to b\bar{b}\ell^+\ell^-$, $HZ \to W^+W^-q\bar{q}$ and $HZ \to W^+W^-\ell^+\ell^-$ channels [17]. As an example Figure 10 demonstrates the distribution of the reconstructed invariant mass of W pair in the channel $HZ \to W^+W^-q\bar{q}$ with subsequent decays of the W bosons into hadrons for 180 GeV Higgs mass and 500 fb^{-1} at 350 GeV. Optimally combining measurements in non-overlapping channels, the Higgs boson mass can be determined with an accuracy of 40 to 70 MeV for Higgs mass ranging from 120 to 180 GeV.

If a signal is detected in a mass spectrum, the measurement of the spin and CP quantum numbers of the observed particle is crucial for its identification as the Higgs boson. It can be performed by analyzing the energy dependence of the Higgs boson production cross section just above the kinematic

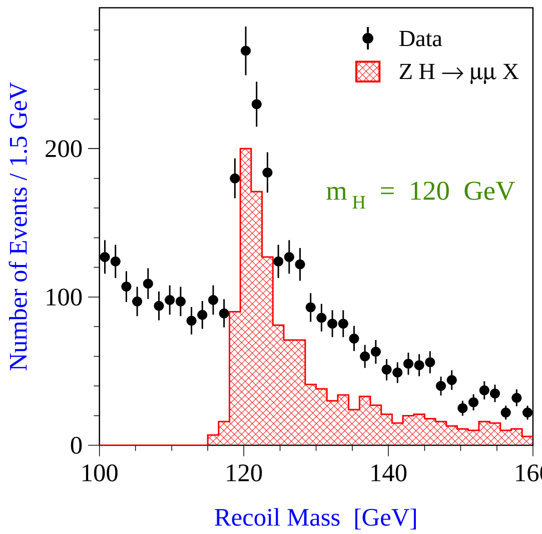

Figure 9: The $\mu^+\mu^-$ recoil mass distribution in the process $e^+e^- \to HZ \to \mu^+\mu^-X$ for 120 GeV Higgs mass and 500 fb^{-1} at 350 GeV. The dots with error bars are Monte Carlo simulation of Higgs signal and background. The shaded histogram represents the signal only.

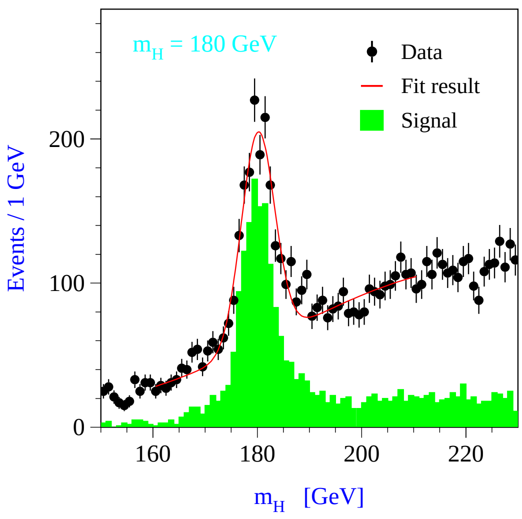

Figure 10: The distribution of the reconstructed Higgs boson mass in the $HZ \to W^+W^-q\bar{q}$ channel with subsequent hadronic decays of the W bosons. The dots with error bars are Monte Carlo simulation of Higgs signal and background. The shaded histogram represents the signal only.

threshold [18]. For a spin zero particle the rise of the cross section is expected to be $\sim \beta$, where β is the velocity of the boson in the center-of-mass system [2]. For a spin one particle the rise is $\sim \beta^3$ and for spin two like $\sim \beta^5$. With a very small luminosity of about 20 fb^{-1} per energy point the scalar nature of the Higgs boson can be established and other spin hypotheses are disfavored, as shown in Figure 11.

The Higgs boson parity can be established in various complementary ways. One of them is based on the analysis of the spin correlation effects in the Higgs boson decay into fermion pairs [19]. The spin dependence of the decay probability is given by

$$\Gamma(H, A \to f\bar{f}) \sim 1 - s_z\bar{s}_z \pm s_\perp\bar{s}_\perp,$$

where s and $\bar{s}$ denote spin vectors of of fermion f and antifermion $\bar{f}$ in their respective rest frames (z axis oriented in the fermion flight direction). Positive sign in the transversal spin correlation term holds for the scalar particle (H) whereas negative sign for the pseudoscalar one (A). Although the dominant fermionic decay mode of the Higgs boson is into b quark pairs it can hardly be utilized for measurement of the Higgs parity, as hadronisation of quarks will inevitably dilute the spin information. The most promising channel is the Higgs decay into tau leptons, with their subsequent decay into ρ meson and neutrino [20]. The angle between planes spanning between products of the $\rho^+ \to \pi^+\pi^0$ and $\rho^- \to \pi^-\pi^0$ decays in the $\rho^+\rho^-$ rest frame clearly distinguishes between the scalar and pseudoscalar states as illustrated in Figure 12. Alternatively, if statistics in the $H \to \tau^+\tau^-$ is not sufficient, the Higgs boson CP-quantum numbers can determined from the study of the polar production angle of the Higgs boson in the Higgs-strahlung process [21, 22].

The width of the Higgs boson, Γ_H, is of several GeV for masses $m_H > 250$ GeV and detector performance allows to measure it directly from the invariant mass spectra [23]. At lower masses, however, the detector resolution is much larger than Γ_H. But using the relation

$$\Gamma_H = \frac{\Gamma(H \to X)}{Br(H \to X)}$$

[2] There are particular scenarios for s=1 and 2, which show a threshold behavior similar in shape to the s=0 one. This can be disentangled using angular information in addition.

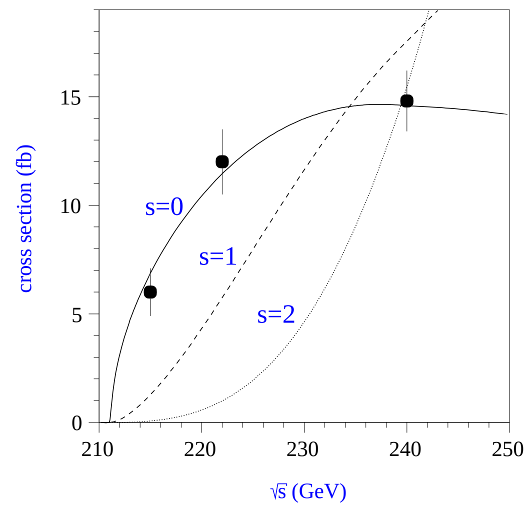

Figure 11: The cross section of $HZ \to q\bar{q}\ell^+\ell^-$ just above the threshold assuming $m_H = 120$ GeV. The dots correspond to a measurement and the curves are predictions for several spins.

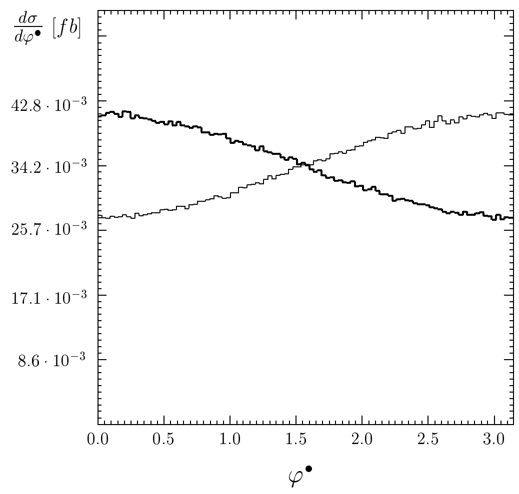

Figure 12: The $\rho^+\rho^-$ decay products' acoplanarity angle, ϕ^* distribution in the rest frame of the $\rho^+\rho^-$ pair. Detector smearing is included. Thick line denote the case of the scalar Higgs boson and thin line the pseudoscalar one. Units valid for 500 GeV center-of-mass energy and Higgs mass of 120 GeV.

with $X = ZZ$, W^+W^- or $\gamma\gamma$ the width can be determined indirectly. For example, the partial width $\Gamma(H \to \gamma\gamma)$ can be measured with a $\gamma\gamma$ collider [24, 25] whereas the branching fraction $Br(H \to \gamma\gamma)$ is accessible in e$^+$e$^-$ collider from the diphoton invariant mass spectrum [26]. The same procedure can be performed for WW fusion process and $H \to WW$ decay mode [27]. Depending on m_H the accuracy in determination of Γ_H between 4% and 10% can be reached.

Finally, unambiguous establishment of the Higgs mechanism implies the complete reconstruction of the Higgs potential. The measurement of the trilinear Higgs coupling will here play a crucial role. This coupling can be determined by measuring the double Higgs boson production cross-section $e^+e^- \to HHZ$ at higher collider energies. It has been shown [28] that trilinear Higgs coupling can be measured with a statistical accuracy of 22% for $m_H = 120$ GeV with an integrated luminosity of 1000 fb^{-1} collected at the center-of-mass energy of 800 GeV.

5.2 Supersymmetry

Supersymmetry (SUSY) is a tempting concept which overcomes several conceptual inconsistencies of the minimal Standard Model. Firstly, it solves the so-called "hierarchy problem" and stabilizes radiative loop corrections to the Higgs boson mass. Being realized locally, SUSY incorporates gravity in a natural way as a quantum field theory. Finally, with the particle content of the supersymmetric models, the running couplings describing gauge interactions meet precisely at one point at the scale of $\sim 10^{15}$-10^{16} thus indicating unification of the strong, electromagnetic and weak interactions. In the minimal supersymmetric extension of the Standard Model (MSSM), each SM particle acquires a superpartner differing in spin by half a unit, e.g. the SM fermions of the SU(2) doublet or singlet are supplemented by scalar fermions (sfermions) whereas the SM gauge bosons are assigned spin 1/2 particles denoted gauginos. The Higgs sector of CP-conserving SUSY models contains at least two Higgs doublets, resulting in 5 physical states: two CP-even bosons h, H, one CP-odd boson A and two charged bosons $H^\pm$. The Higgs bosons have superpartners called higgsinos. The sfermion sector comprises left- and right-handed superpartners of the SM fermion fields. A large mixing between left- and right fields occurs in the third fermion generation, giving rise to a large mass splitting between mass eigenstates of stau leptons $\tilde{tau}_{1,2}$, sbottom $\tilde{b}_{1,2}$ and stop quarks $\tilde{t}_{1,2}$. The non-strongly interacting gauginos mix with the higgsinos to form corresponding mass eigenstates: two pairs of charginos $\tilde{\chi}_i^{\pm}$ (i = 1,2) and four neutralinos $\tilde{\chi}_i^0$ (i = 1..4). In the MSSM the multiplicative quantum number R-parity is conserved, R_p = +1 for SM particles and R_p = -1 for the supersymmetric partners. This implies existence of a lightest supersymmetric particle (LSP), which is stable and to which all supersymmetric particles eventually decay. In most of the models the lightest neutralino $\tilde{\chi}_1^0$ is assumed to be LSP. The fact that supersymmetric particles have not been detected so far indicates that SUSY is broken and supersymmetric particles have higher masses than their SM partners. Several models have been proposed to describe dynamics of the SUSY breaking and introduce new parameters into the theory. As an example Figure 13 shows the mass spectrum of SUSY particles for the SPS 1a benchmark point of the minimal supergravity (mSUGRA) scenario [29, 30].

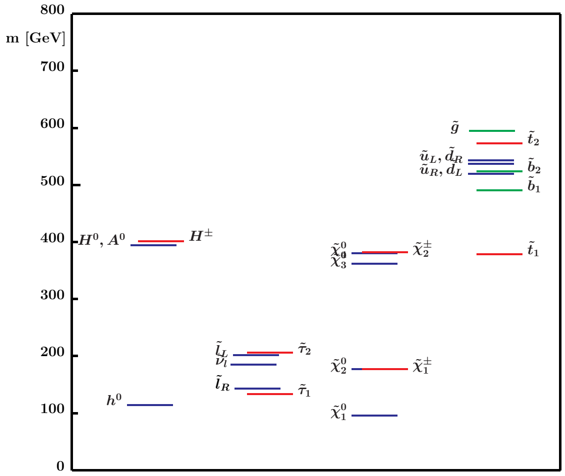

Figure 13: The mass spectrum of SUSY particle corresponding to the SPS 1a benchmark point of the minimal supergravity (mSUGRA) scenario.

If low energy supersymmetry is discovered at LHC, its fundamental features can be revealed, in particular in the strongly interacting squark and gluino sector. However, given the fact that many SUSY particles are expected to be within the energy reach of the linear collider, the latter will be indispensable in order to provide complementary information in the slepton and gaugino sectors. Beam polarization will be vital for disentangling various SUSY processes from the background. It is generally assumed that polarizations of 80 and 60% are feasible for electron and positron beams. The potential of the ILC for exploring SUSY can illustrated using as an example the SPS 1a benchmark point.

Scalar leptons are produced in e$^+$e$^-$ collisions in pairs

$$e^+e^- \rightarrow \tilde{\ell}_i^+\tilde{\ell}_j^-, \tilde{\nu}\bar{\tilde{\nu}}$$

via s-channel Z/γ exchange or t-channel $\tilde{\chi}$ exchange for the first generation. The left-handed and right-handed states can be determined using beam polarization, e.g. $\tilde{\ell}_R\tilde{\ell}_R$ production has much larger cross section for right-handed electrons than for left-handed. Positron polarization further enhances the effect. The isotropic two-body decays

$$\tilde{\ell}^- \rightarrow \ell^-\tilde{\chi}_i^0, \qquad \tilde{\nu}_\ell \rightarrow \ell^-\tilde{\chi}_i^+$$

lead to a uniform lepton energy spectrum with minimal and maximal energy edges (”endpoints”). From the kinematic ”endpoints” the masses of the primary slepton and the secondary chargino/neutralino can be measured. Figure 14 shows an example of the reconstructed muon energy in the $e_L^+e_R^- \rightarrow \tilde{\mu}_R^+\tilde{\mu}_R^- \rightarrow \mu^+\tilde{\chi}_1^0\mu^-\tilde{\chi}_1^0$ process [31]. In this case masses of smuon and lightest neutralino can be measured with the precision of about 0.2 GeV, assuming 200 fb^{-1} at center-of-mass energy of 400 GeV. Higher accuracy ($\sim$ 0.1 GeV) can be achieved by measuring the slepton pair production cross section in the vicinity of the kinematic threshold [1].

Charginos and neutralinos are produced in pairs

$$e^+e^- \rightarrow \tilde{\chi}_i^+\tilde{\chi}_j^-, \qquad e^+e^- \rightarrow \tilde{\chi}_i^0\tilde{\chi}_j^0$$

via s-channel Z/γ exchange and t-channel $\tilde{e}$ and $\tilde{\nu}_e$ exchange and decay into lighter partners and gauge bosons or sfermion-fermion pairs

$$\tilde{\chi}_i \rightarrow Z/W\tilde{\chi}_j, \qquad \tilde{\chi}_1^{\pm} \rightarrow \tilde{\tau}^{\pm}\nu_\tau \rightarrow \tau^{\pm}\nu_\tau\tilde{\chi}_1^0, \qquad \tilde{\chi}_2^0 \rightarrow \tilde{\ell}\ell \rightarrow \ell\ell\tilde{\chi}_1^0.$$

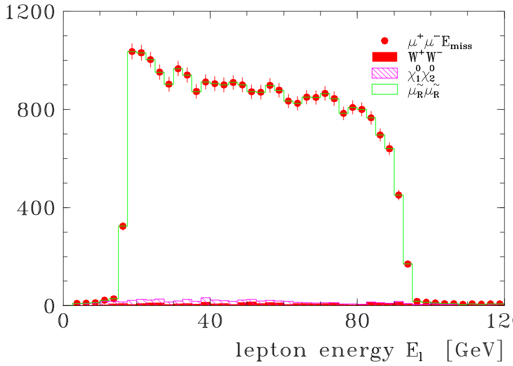

Figure 14: The spectrum of muon energy in the reaction $e^+_L e^-_R \to \tilde{\mu}^+_R \tilde{\mu}^-_R \to \mu^+ \tilde{\chi}^0_1 \mu^- \tilde{\chi}^0_1$ for SPS 1a benchmark point. Center-of-mass energy is 400 GeV. Integrated luminosity is 200 fb^{-1}.

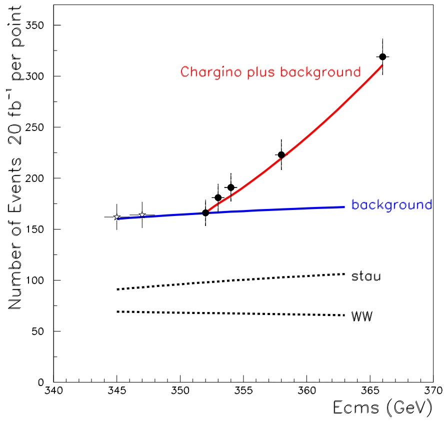

Figure 15: Threshold scan of $e^+_R e^-_L \to \tilde{\chi}^+ \tilde{\chi}^- \to \tau^+ \nu_\tau \tilde{\chi}^0_1 \tau^- \bar{\nu}_\tau \tilde{\chi}^0_1$ for the SPS 1a point assuming 20 fb^{-1} of integrated luminosity at each scan point.

The most promising method to measure the lightest chargino and the next to the lightest neutralino masses is the threshold scan. Figure 15 shows as an example the number of selected events compatible with the $e^+_R e^-_L \to \tilde{\chi}^+_1 \tilde{\chi}^-_1 \to \tau^+ \nu_\tau \tilde{\chi}^0_1 \tau^- \bar{\nu}_\tau \tilde{\chi}^0_1$ topology as a function of center-of-mass energy around the $\tilde{\chi}^+_1 \tilde{\chi}^-_1$ production threshold. With only five scan points and luminosity of 20 fb^{-1} per point, the light chargino mass can be measured with the statistical precision of 0.55 GeV [1]. The next $\tilde{\chi}^0_2$ mass can be measured by threshold scan of $e^+_R e^-_L \to \tilde{\chi}^0_2 \tilde{\chi}^0_2 \to 4\tau + 2\tilde{\chi}^0_1$. With an integrated luminosity of 100 fb^{-1} distributed over five scan points, the precision on the mass of 1.2 GeV can be achieved. The heavy chargino and neutralinos can be detected via their associated production with the lighter ones, followed by the decay $\tilde{\chi}_j \to W/Z\tilde{\chi}_i$. The expected accuracy of the mass measurement of a few GeV is feasible [32].

Charginos are the mixture of Winos and Higgsinos. The Wino component is accessible via chargino pair production via t-channel exchange, which couples only to left-handed electrons. Hence, the mixing parameters in chargino sector can be measured by varying beam polarization [33]. By measuring mixing in the chargino sector one gets an access to the fundamental supersymmetric parameters, namely gaugino mass parameter M_2, Higgs mixing parameter μ and the ratio of the vacuum expectation value of the two Higgs doublets, $\tan\beta$. In a similar way the properties of neutralino system, which is the mixture of Bino, Wino and two Higgsinos, can be determined. By measuring the dependence of neutralino pair production on the beam polarization, in addition to the parameters M_2, μ and $\tan\beta$, the gaugino mass parameter M_1 can be extracted [1].

Light stop production may become accessible at the ILC operated at $\sqrt{s} = 1$ TeV. The observation will be based on the production and decay sequence $e^+e^- \to \tilde{t}_1 \bar{\tilde{t}}_1 \to b\tilde{\chi}^+_1 \bar{b}\tilde{\chi}^-_1 \to b\tau^+\bar{\nu}_\tau \tilde{\chi}^0_1 \bar{b}\tau^-\nu_\tau\tilde{\chi}^0_1$. One can then use the energy spectrum of the b-jets and exploit $b\bar{b}$ correlations to construct the minimum kinematically allowed visible mass assuming the mass of $\tilde{\chi}^\pm_1$ to be known [34]. With a luminosity of 1000 fb^{-1} the rate will be sufficient to achieve a precision on the light stop mass of 2 GeV.

As was already mentioned above, the Higgs sector of the supersymmetric models consists at least of five physical states. Within the SPS 1a benchmark scenario the light neutral CP-even state has a mass of 114 GeV while the heavy states are almost degenerate in mass, $m_A = 393.6$ GeV, $m_H = 394.1$ GeV, and decoupled from the gauge bosons. The H and A bosons can be detected via their associated production process, $e^+e^- \to HA$, followed by $H, A \to b\bar{b}$. Exploiting excellent b-tagging capabilities and good jet energy resolution, envisaged for the linear collider detector, the $HA \to b\bar{b}b\bar{b}$ final states can be efficiently reconstructed and the heavy Higgs boson masses can be measured with an accuracy of a few GeV [35] assuming 1000 fb^{-1} of an integrated luminosity at $\sqrt{s} = 1$ TeV. The reconstructed Higgs boson mass sum spectrum is illustrated in Figure 16. Charged Higgs boson are produced in e$^+$e$^-$ collisions in pairs and can be detected via $H^+ \to t\bar{b}$, $H^+ \to \tau^+\bar{\nu}_\tau$ or $H^+ \to W + h$ decay modes, giving rise to various signatures, ranging from the topology with two narrow jets and missing energy ($H^+H^- \to \tau^+\bar{\nu}_\tau\tau^-\nu_\tau$) to eight jet final states ($H^+H^- \to W^+hW^-h/t\bar{b}\bar{t}b \to 8jet$).

The physical observables, such as slepton and gaugino masses, mixing angles in the chargino and neutralino sector *etc*, can be translated into fundamental SUSY Lagrangian parameters through the theoretical relations including loop corrections. Conversion of the observable quantities into fundamental SUSY Lagrangian parameters and proper errors propagation can be done using currently available software which performs global fits in the SUSY sector [36, 37]. In their turn, fundamental parameters can be evolved to the higher energy scales and the hypothesis of Grand Unification can be verified. This is illustrated in Figure 17 for gaugino mass parameters M_1, M_2 and M_3. For the SPS 1a scenario in mSUGRA three curves, indicating dependence of gaugino mass parameters on the energy scale Q, meet at one point at $Q \sim 10^{16}$ GeV, thus pointing to the unification of gauge interactions.

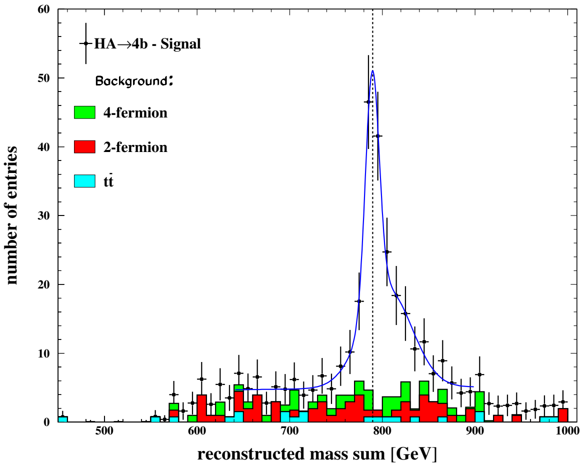

Figure 16: The reconstructed Higgs boson mass sum, $m_H + m_A$ in the $HA \to b\bar{b}b\bar{b}$ channel assuming 1000 fb^{-1} at $\sqrt{s} = 1$ TeV.

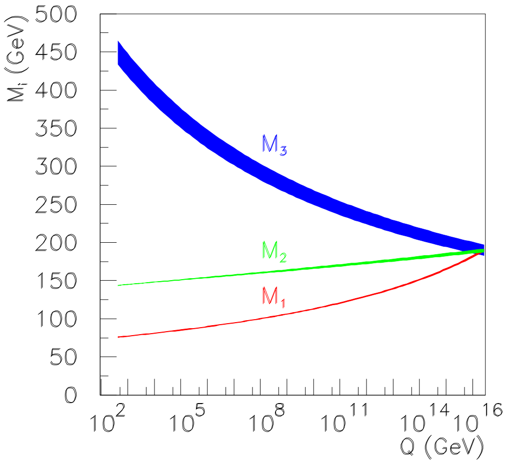

Figure 17: Evolution of the gaugino mass parameters M_1, M_2 and M_3 with the energy scale in mSUGRA scenario. The bands indicate 95% CL contours.

5.3 Spatial Extra Dimensions

Novel theoretical ideas which exploit the geometry of extra spatial dimensions have been proposed over recent years in order to explain the large hierarchy between electroweak and gravity scales. In the scenario of Arkani-Hamed, Dimopoulos and Dvali (ADD model) [38] the apparent hierarchy is generated by a large volume of the compactified extra dimensions. Gravitational interactions become strong near the weak scale and take place mainly in δ new large spatial dimensions, known as the bulk. Since the Standard Model fields are experimentally found to be insensitive to the effects of extra dimensions with compactification scales less than a few TeV, they are constrained to lie on a $3+1-$ dimensional brane. The relation between the scales where gravity becomes strong in the $4+\delta$ and $4-$ dimensional theories can be derived from Gauss's Law and is given by $M_{Pl}^2 = V_\delta M_D^{2+\delta}$, where M_D denotes the fundamental Planck scale in the higher dimensional space, V_δ is the volume of the compactified extra dimensions. The bulk gravitational fields in this scenario manifest themselves as the spectrum of excitation states, called Kaluza-Klein towers of gravitons [39]. These states have the masses given by the formula $m_{KK}(n) = n/R$, where R is the radius of compactified extra dimensions. For $M_D \sim 1$ TeV, KK state mass splitting is $5{\cdot}10^{-4}$ eV, 20 keV and 7 MeV for $\delta = 2$, 4 and 6, respectively. There are two ways in which gravity may manifest itself at the linear e$^+$e$^-$ collider. The first one is the graviton emission in the scattering process, $e^+e^- \to \gamma/Z + G_n$, where the graviton appears as missing energy in the detector. The cross section of the graviton emission is obtained by summing over the full tower of KK states. The discovery reach of the TESLA collider for direct graviton production is evaluated for the process $e^+e^- \to \gamma G$ assuming an integrated luminosity of 1 ab^{-1} at $\sqrt{s} = 800$ GeV [40]. Beam polarization is crucial in this analysis for disentangling signal from various background processes, e.g. $e^+e^- \to \nu\bar{\nu}\gamma$. Extra dimensions would be signaled by the anomalous single photon production cross section. The TESLA sensitivity in mass scale M_D for different values of δ and different beam polarizations is presented in Table 2.

If extra dimensions are the cause of the anomalous single photon production rate, the energy dependence of the cross-section should follow $\sigma(\sqrt{s})^\delta$. Complementing measurement of the single photon production cross section at $\sqrt{s}$ = 800 GeV with a similar measurement at lower energy, for instance $\sqrt{s}$ = 500 GeV, the number of extra dimensions can be determined. This is illustrated in Figure 18.

The second way to probe ADD model at the linear e$^+$e$^-$ collider is through virtual effects associated with the graviton exchange in 2→2 scattering [39, 41]. The mass scale M_D can be probed by measuring the cross section and forward-backward asymmetry of fermion-antifermion production as a function of the polar production angle of fermions. Table 3 summarizes the sensitivity in M_D for virtual effects in $\mu^+\mu^-$, $b\bar{b}$ and $c\bar{c}$ production [42].

$\delta =$	2	3	4	5	6
$P_{-,+} = 0$	5.9	4.4	3.5	2.9	2.5
$P_- = 0.8$	8.3	5.8	4.4	3.5	2.9
$P_- = 0.8$, $P_+ = 0.6$	10.4	6.9	5.1	4.0	3.3

Table 2: Sensitivity (95% CL) in M_D in TeV for direct graviton production $e^+e^- \to \gamma G$ for various values of δ and different beam polarizations.

$\sqrt{s} =$	500 GeV	800 GeV
$e^+e^- \to \mu^+\mu^-$	4.1	5.8
$e^+e^- \to b\bar{b}$	5.0	7.1
$e^+e^- \to c\bar{c}$	5.1	7.1
combined	5.6	8.0

Table 3: Sensitivity (95% CL) in M_D in TeV for indirect effects in $\mu^+\mu^-$, $b\bar{b}$ and $c\bar{c}$ production. An integrated luminosity of 500 fb^{-1} is assumed for $\sqrt{s}$ = 500 and 1 ab^{-1} for $\sqrt{s}$ = 800 GeV, respectively.)

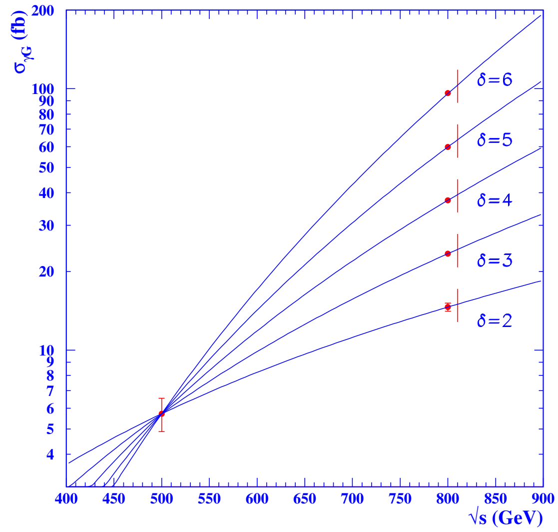

Figure 18: Determining δ from anomalous single photon production cross-section measurements at $\sqrt{s}$ = 500 and 800 GeV. The sensitivity shown corresponds to integrated luminosities of 500 fb^{-1} is assumed for $\sqrt{s}$ = 500 and 1 ab^{-1} for $\sqrt{s}$ = 800 GeV, respectively with 80% electron and 60% positron polarizations.

Another approach of addressing the issue of large hierarchy between electroweak and Planck scales is offered by Randall and Sundrum [43]. In their model, the observed hierarchy is created by exponential warp factor which arises from the localization of gravity in a 5-dimensional non-factorizable geometry with the metric $ds^2 = e^{-2kr_c}\eta_{\mu\nu}dx^\mu dx\nu - r_c^2 d\phi^2$, where $0 \leq |\phi| \leq \pi$ is the coordinate of an extra dimension, which is a finite interval whose size is set by r_c. The parameter k is the AdS$_5$ curvature scale which is of the order of the Planck scale and is determined by the bulk cosmological constant $\Lambda_5 = -24M_5^3k^2$, where M_5 is the 5-dimensional Planck scale. The effective 4-dimensional Planck scale is related to M_5 and k via $\bar{M}_{Pl}^2 = (1 - e^{-2kr_c})M_5^3/k$. TeV scales can be naturally obtained on the 3-brane at $\phi = \pi$ if gravity is localized on the Planck scale at $\phi = 0$ and $kr_c \sim 10$. The scale of physics processes on the visible 3-brane at $\phi = \pi$ is then $\Lambda_\pi \equiv \bar{M}_{Pl}e^{-kr_c\pi} \sim$ TeV. The 4-dimensional phenomenology of this model is governed by two parameters, Λ_π and the ratio $k/\bar{M}_{Pl}$. The model predicts KK tower of gravitons with masses given by $m_n = x_n k e^{-kr_c\pi}$ with x_n being the roots of the first-order Bessel function. It should be noted that the first excitation is naturally of the order of a few hundred GeV and the KK states are not equally spaced. Due to the explicit form of the interactions of the KK tower with the Standard Model fields on the visible 3-d brane, the zero mode decouples whereas excitation states couple to fermion fields of the Standard Model with a strength of an inverse TeV and can undergo single, direct production. Consequently, they can be identified at the linear collider via the resonant behavior of the $e^+e^- \to f\bar{f}$ production cross section as illustrated in Figure 19.

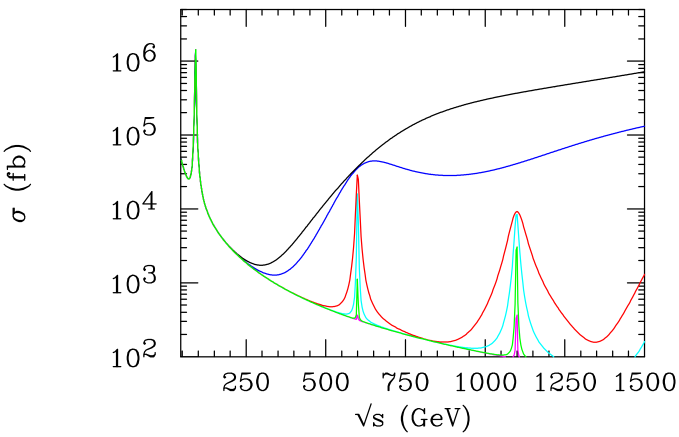

Figure 19: The cross-section for $e^+e^- \to \mu^+\mu^-$ including the exchange of a KK tower of gravitons with $m_1 = 600$ GeV in the Randall-Sundrum model. From top to bottom the curves correspond to $k/\bar{M}_{Pl}$ = 1.0, 0.5, 0.1, 0.05, 0.02 and 0.01.

5.4 Electroweak Symmetry Breaking by Strong Dynamics

In the absence of a light scalar field, new physics coupled to the Standard Model is needed at the TeV scale to preserve the unitarity of the model. In theories of dynamical electroweak symmetry breaking, the electroweak interactions are broken to electromagnetism by non zero vacuum expectation value of a fermion bilinear. Prominent examples include Technicolor, topcolor and related models [44] which conventionally introduce a new non-Abelian gauge group and additional massless fermions, "technifermions", which feel the force associated with the new group. The global chiral symmetry of the fermions is broken by the formation of the fermion condensate. This resembles the symmetry breaking pattern of GCD in the limit of zero quark masses. The breaking of global chiral symmetries implies the existence of Goldstone bosons. In Technicolor models, the pions of the new strong symmetry, called "technipions", play the role of Goldstone bosons. Through the Higgs mechanism, three Goldstone bosons become longitudinal components of W and Z and the weak gauge bosons acquire a mass proportional to technipion decay constant (the analog of f_π in QCD). The spectrum of remaining physical states is model dependent.

If the new strong dynamics scale is somewhat higher than 1 TeV, the expected signature would be enhanced gauge boson self-interactions, conventionally parameterized by "anomalous" couplings. The models of strong dynamics can therefore be verified via the measurements of the "anomalous" triple gauge boson couplings exploiting the process $e^+e^- \to W^+W^-$ [45]. Using polarized beams would improve precision of these measurements and consequently enhance the sensitivity to the energy scales associated with the new strong dynamics. Other effective probe of the strong electroweak symmetry breaking is provided by the scattering of a pair of longitudinally polarized weak gauge bosons at high center-of-mass energies ($\sqrt{s} = 0.8 - 1$ TeV). By measuring the change of the event rate and of the average polarization of the gauge bosons with respect to the SM in the six-fermion final states $e^+e^- \to WW(ZZ)\nu\bar{\nu} \to q\bar{q}q\bar{q}\nu\bar{\nu}$ one gets access to the "anomalous" quartic gauge couplings and therefore probes the new strong dynamics affecting dimension-four operators describing gauge boson self-interactions [46]. Again beam polarization will be crucial for these measurements.

6 Conclusion

A future linear e^+e^- collider opens broad perspectives for high energy physics, providing a perfect tool for the detailed exploration of the electroweak symmetry breaking mechanism. The high energy reach of such a machine will enable physicists to search also for new physics phenomena such as supersymmetry and extra spatial dimensions. An extensive international R&D program is currently underway which aims to establish technologies and design detector components in the most optimal way in order to reach the detector performance goals required by the planned physics program. A number of test-beam experiments which will test various sub-detector prototypes, such as electromagnetic and hadron calorimeters, TPC and a tail catcher/muon system, will be carried out in the nearest future. Results of these experiments will allow to further optimize a detector foreseen for the e^+e^- collider. As a final remark, it should be emphasized that this project is unlikely to be realized by some country or region alone, and can come fruitful only as a result of a world-wide global effort.

References

[1] F. Richard, J.R. Schneider, D. Trines and A. Wagner, *"TESLA : Technical Design Report"*, DESY 2001-01, ECFA 2001-209, TESLA Report 2001-023, TESLA-FEL 2001-05 (2001)

[2] American Linear Collider Working Group, *"Linear Collider Physics"*, BNL-52627, CLNS 01/1729, SLAC-R-570, FERMILAB-Pub-01/058-E, LBNL-47813, UCRL-ID-143810-DR, LC-REV-2001-074-US (2001).

[3] Asian Comittee for Future Accelerators, Japan High Energy Physics Comittee, High Energy Accelerator Research Organisation, GLC Project (2003).

[4] ILC-TRC/2003 Report, http://www.slac.stanford.edu/xorg/ilc-trc/2002/2002/report/03rep.htm.

[5] K.Desch, A.Imhof, N.Meyer, A.Raspereza, LC-PHSM-2004-009.

[6] ITRP Final Report, http://www.ligo.caltech.edu/~skammer/ITRP_Home.htm.

[7] C. J. Damerell *et al.*, SLAC-REPRINT-1996-009 (1996)

[8] T.Kuhl, Nucl.Instrum.Meth. **A511** (2003) 221

[9] S.M. Xella-Hansen *et al.*, Nucl.Instrum.Meth. **A501** (2003) 106

[10] J. Hauschild, LC-DET-2001-036.

[11] V. Morgunov, A. Raspereza, *"Novel 3D Clustering Algorithm and Two Particle Separation with Tile HCAL"*, Proceedings of the International Conference on Linear Colliders, LCWS 2004, Paris 2004, physics/0412108.

[12] V. Andreev *et al.*, LC-DET-2004-027, DESY-04-143 (2004), submitted to Nucl. Instr. Meth.

[13] V. Morgunov, *"Calorimetry Design Wwith Energy Flow Concept (Imaging Detector for High Energy Physics)"*, 10th International Conference on Calorimetry in High Energy Physics (CALOR 2002), Pasadena, California, 25-30 Mar 2002, published in Pasadena 2002, "Calorimetry in particle physics" 70-84.

[14] V. Morgunov, SNARK package, available at www-zeuthen.desy.de/lc_repository/detector_simulation/dev/BRAHMS/tex/snark_html/index.html

[15] S. Chekanov and V. Morgunov, Phys.Rev. **D67** (2003) 074011

[16] P. Garcia-Abia W. Lohmann, EPJdirect **C2** (2000) 1

[17] P. Garcia-Abia, W. Lohmann, A. Raspereza, LC-PHSM-2000-062, AIP Conference Proceedings, 578-1 (2001) 218

[18] M.T. Dova, P. Garcia-Abia, W. Lohmann, LC-PHSM-2001-055, hep-ph/0302113.

[19] S.Y. Choi, D. Miller, M. Muhlleitner and P. Zerwas, Phys.Lett. **B553** (2003) 61

[20] G.R. Bower, T. Pierzchala, Z. Was, M. Worek, Phys.Lett. **B543** (2002) 227

[21] M. Schumacher, LC-PHSM-2001-003.

[22] M.T. Dova, S. Ferrari, hep-ph/0406313.

[23] N. Meyer, K. Desch, Eur.Phys.J. **C35** (2004) 171

[24] P. Niezurawski, A.F. Zarnecki and M. Krawczyk, Acta Phys.Polon. **B34** (2003) 177

[25] A. Rosca, K. Moenig, LC-PHSM-2003-084.

[26] E. Boos *et al.*, Eur.Phys.J. **C19** (2001) 455

[27] N. Meyer, K. Desch, LC-PHSM-2001-025.

[28] C. Castanier, P. Gay, P. Lutz, J. Orloff, LC-PHSM-2000-061, hep-ex/0101028.

[29] B.C. Allanach *et al.*, Eur.Phys.J. **C25** (2002) 113

[30] N. Ghodbane, H.U. Martyn, hep-ph/0201233.

[31] H.U. Martyn, LC-PHSM-2003-071.

[32] U. Nauenberg, talk at ECFA/DESY LC Workshop Prague, November 2002, http://www-hep2.fzu.cz/ecfadesy/Talks/SUSY.

[33] S. Choi *et al.*, Eur.Phys.J. **C14** (2000) 535;
G. Moortgat-Pick, A. Bartl, H. Fraas, W. Majerotto, LC-TH-2000-033.

[34] J. Feng, D. Finell, Phys.Rev. **D49** (1994) 2369

[35] K. Desch, T. Klimkovich, T. Kuhl and A. Raspereza, LC-PHSM-2004-006, hep-ph/0406229.

[36] R. Lafaye, T. Plehn and D. Zerwas, LAL 04-06, LAPP-EXP-2003-27, CERN-TH/2003-312 (2003), http://sfitter.web.cern.ch/SFITTER.

[37] P. Bechtle, K. Desch, P. Wienemann, hep-ph/0412012, submitted to Comp.Phys.Commun.;
P. Bechtle, *"SUSY Higgs Boson Searches at LEP and SUSY Parameter Measurements at TESLA"* PhD thesis, University of Hamburg, DESY-THESIS-2004-040 (2004);
http://www-flc.desy.de/fittino.

[38] N. Arkani-Hamed, S. Dimopoulos, G. Dvali, Phys.Lett. **B429** (1998) 263

[39] G.F. Giudice, R. Rattazzi, J.D. Wells, Nucl.Phys. **B544** (1999) 3;
T. Han, J. Lykken, R.J. Zhang, Phys.Rev. **D59** 105006 (1999)

[40] G.W. Wilson, LC-PHSM-2001-010;
A. Vest, LC-TH-2000-058.

[41] J.L. Hewett, Phys.Rev.Lett. 82 (1999) 4765;
T.G. Rizzo, Phys.Rev. **D59** (1999) 115010

[42] S. Riemann, LC-TH-2001-007

[43] L. Randall, R. Sundrum, Phys.Rev.Lett. 83 (1999) 3370;
L. Randall, R. Sundrum, Phys.Rev.Lett. 83 (1999) 4690

[44] S. Weinberg, Phys.Rev. **D20** (1979) 1277;
L. Susskind, Phys.Rev. **D20** (1979) 2619;
K. Lane, hep-ph/0007304;
E.H. Simmons, hep-ph/0110196.

[45] W. Menges, LC-PHSM-2001-022.

[46] R. Chierici, S. Rosati, M. Kobel, LC-PHSM-2001-038.